Carbohydrate Polymers 180 (2018) 55–62

Contents lists available at ScienceDirect

Carbohydrate Polymers

journal homepage: www.elsevier.com/locate/carbpol

Research Paper

Application of chitosan in removal of molybdate ions from contaminated water and groundwater

Fernando A. Bertoni[a,b], Juan C. González[a,b], Silvia I. García[a,b], Luis F. Sala[a,b], Sebastián E. Bellú[a,b,*]

[a] Área Química General e Inorgánica, Departamento de Química-Física, Facultad de Ciencias Bioquímicas y Farmacéuticas, Universidad Nacional de Rosario, Suipacha 531, S2002LRK Rosario, Santa Fe, Argentina
[b] Instituto de Química de Rosario-CONICET, Suipacha 570, S2002LRK Rosario, Santa Fe, Argentina

ARTICLE INFO

Keywords:
Adsorption
Chitosan
Molybdenum
Groundwater

ABSTRACT

Water pollution by heavy metals represents a serious problem around the world. Among various treatment techniques for water remediation, adsorption is an effective and versatile method due to the low cost, effectiveness and simplicity. Chitosan is a cationic polysaccharide with an excellent adsorption capacity of heavy metal ions. Chitosan has a high molybdate adsorption capacity (265 ± 1 mg g^{-1}) at 20 °C and pH 2.7. Participation of hydroxyl groups in the adsorption of molybdate anions was confirmed by FT-IR analysis. SEM images showed that morphological surface changes happen after Mo^{VI} adsorption. Continuous adsorption data were best fitted by Modified Dose- Response model. Scale-up of continuous processes was achieved applying bed depth service time (BDST) model. Application of chitosan in molybdate removal from real groundwater samples suggest that this polysaccharide is a good option to be used for household purposes.

1. Introduction

Heavy metal contamination represents a major problem around the world due to industrial wastewaters discharged into natural water bodies (Fu & Wang, 2011). Some water purification processes have been applied to wastewaters including adsorption, electrolytic chemical treatment, membrane separation, and biological treatment. From these techniques, adsorption has some advantages such as low cost, effectiveness and simplicity.

Chitosan is a cationic polysaccharide (poly[β-(1 → 4)-2-amino-2-deoxy-D-glucopyranose]) partially acetylated at the 2-amino group. It is obtained by deacetylation of chitin (poly[β-(1 → 4)-2-acetamido-2-deoxy-D-glucopyranose]), which is a natural polysaccharide component of arthropod and crustacean shells (Guibal, 2004). Chitosan is soluble in acetic acid, and insoluble in dilute sulfuric acid. Presence of free amino and hydroxyl group in its structure confers to this polysaccharide an excellent adsorption capacity of heavy metal ions (Li et al., 2016). The low cost, non-toxic and biodegradable properties combined to its high adsorption capacity of heavy metals makes this polysaccharide an excellent option to be used in treatment of polluted effluents.

Molybdenum is a trace element that is present in plants and animals (Gupta, 1997). It is harmful to plants at concentration higher than 5 μg g^{-1}, and for ruminants at concentration higher than 10 μg g^{-1} (Goldberg, Lesch, & Suarez, 2002). Molybdenum is a second row transition element which has various industrial applications such as constituent of electron and vacuum tubes, fireproof thermal materials and hardness steel alloys (Bei et al., 2007). Pollution by molybdenum species in water bodies and groundwater becomes a serious danger to general population (Smedley, Nicolli, Macdonald, Barros, & Tullio, 2002). Water soluble molybdenum derived anions cause a negative environmental impact if their concentration exceeds 5 mg L^{-1} (Moret & Rubio, 2003). As consequence, the search for water remediation process becomes very challenging.

Chitosan polymers was currently used as adsorbent of arseniate anions (Kumar & Jiang, 2016), lead ions (Mallakpour & Madani, 2016), chromate anions (Hua, Zhang, Bai, Lu, & Liang, 2017) and vanadium oxyanions (Padilla-Rodriguez et al., 2015). So, this polysaccharide is a promising sorbent for remediation processes of polluted waters.

The goal of this study was the application of chitosan biopolymers as a sorbent for Mo^{VI} removal. Since this polysaccharide is abundant in nature and has a low cost of preparation, it has been selected as a possible biosorbent for molybdate removal from contaminated waters. The results obtained demonstrate the ability of chitosan to remove Mo^{VI} from water and support further implementation of the system to decontaminate water at higher scale.

* Corresponding author at: Universidad Nacional de Rosario, Facultad de Ciencias Bioquímicas y Farmacéuticas, Suipacha 531, S2002LRK Rosario, Santa Fe, Argentina.
E-mail addresses: bellu@iquir-conicet.gov.ar, sbellu@fbioyf.unr.edu.ar (S.E. Bellú).

http://dx.doi.org/10.1016/j.carbpol.2017.10.027
Received 5 June 2017; Received in revised form 25 August 2017; Accepted 5 October 2017
Available online 06 October 2017
0144-8617/

2. Experimental

2.1. Materials

Chitosan (Sigma, p.a.), sodium molybdate dihydrate (Baker, P.a.), acetic acid (Cicarelli, p.a.), sulfuric acid (Cicarelli, 98%), sodium hydroxide (Merck, 99%), 1,2-dihydroxibenzene (Sigma, p.a.), sodium methabisulfite (Cicarelli, p.a.), were employed as received.

MilliQ deionized water was used to prepare aqueous solutions. Chitosan solutions were prepared by dissolving the polysaccharide into 4% w/v acetic acid solution at 50 °C.

2.2. Chitosan characterization

Specific viscosity was determined at 25 °C by an Ostwald-type viscosimeter. Flow times were recorded with a stopwatch with reproducibility ± 0.2 s. Pycnometry technique was used to determine densities of solutions. Chitosan solutions (1.0–5.0 g/L) in 0.10 M acetic acid and 0.2 M NaCl were used in this experiment (Bof, Bordagaray, Locaso, & García, 2015). The experimental value of intrinsic viscosity was 265.5. Chitosan molecular weight (MW) was obtained applying Mark Houwink–Sakurada equation (Roberts & Domszy, 1982) and the value of MW obtained was 360000 ± 100 g/mol.

The determination of degree of acetylation (DA) was performed by first derivative FTIR spectroscopy (Beil, Schamberger, Naumann, Macill, & van Peé, 2012). FT-IR spectrum of chitosan were measured using a Perkin Elmer FT-IR Spectrum One spectrophotometer in the range of 200–4000 cm^{-1} employing CsI pellets. The first derivative IR values at 1383 cm^{-1} (MB1), 1327 cm^{-1} (MB2) and 1163 cm^{-1} (RB) were determined. MB1 correspond to a DA (degree of acetylation) sensitive probe band, in this case, CH— deformation band at 1383 cm^{-1}. MB2 correspond to a DA sensitive probe band, in this case, the amide III band at 1327 cm^{-1} and finally, RB correspond to a DA independent reference band, in this case the bridge oxygen stretching band at 1163 cm^{-1}.

DA was calculated applying Eq. (1) (Beil et al., 2012).

$$\frac{(MB1 + MB2)}{RB} = 0.0156DA + 0.487\% \quad (1)$$

Replacing in Eq. (1) we obtain:

$$\frac{(0.2071 + 0.2012)}{0.4248} = 0.0156DA + 0.487\%$$

DA of chitosan was 30.4% (DDA degree of deacetylation was 69.6%).

Due to determination of DA by FT IR is rough, a method based on ^1H NMR was employed (Abdou, Nagy, & Elsabee, 2008).

For ^1H NMR measurement, 5.0 mg of chitosan was introduced into a 5 mm NMR test tube and further vacuum dried at 50 °C for 3 h. Then, 0.5 mL of 2.0% DCI/D_20 solution was added, and finally the test tube was kept at 70 °C to dissolve the polymer.

The ^1H NMR was collected in a Bruker Avance 300 MHz Digital, NS = 64, SW = 12.98, O1P = 5.5, Temp: 70 °C.

The ^1H NMR spectrum obtained was showed in Fig. S1.

It is reported in literature (Hirai, Odani, & Nakajima 1991) that the peak around at 5.0 ppm is assigned to C1 proton of glucosamine unit in chitosan and the peaks in 3.5–4.5 ppm to C2–C6 protons of glucosamine and *N*-acetylglucosamine units. They also showed that C1 proton of *N*-acetylglucosamine unit appears around 5.2 ppm, (see Fig. S1) obtained from chitosan solution. For the determination of the degree of deacetylation(DDA) the method of Hirai was used (Eq. (2)):

$$DDA\% = \left(1 - \frac{\frac{1}{3}ICH_3}{\frac{1}{6}IH_{2-6}}\right) \times 100 \quad (2)$$

where ICH_3 is the integral intensity of resonance band due to CH_3 residue of N-acetylglucosamine and IH_2–H_6 is the sum of integral intensities of H_2–H_6, protons.

Replacing in Eq. (2) we obtain:

$$DDA\% = \left(1 - \frac{\frac{1}{3}x3}{\frac{1}{6}x(22.1 + 3.1)}\right) \times 100$$

The value of DDA% obtained was 76.2%. According to Abdou et al. (Abdou et al., 2008) NMR was found to be the most reliable method to determine DDA%

pH value at point of zero charge (pHpzc) was determined as described in literature (Bertoni, Medeot, González, Sala, & Bellú, 2015). pHpzc of chitosan was 6.3.

2.3. Chitosan gel beads formation

Chitosan gel beads were prepared by dripping a chitosan solution (4% w/v in acetic acid) into a 2.5 M NaOH solution. Freshly prepared chitosan gel beads were left 24 h into NaOH solution and then were separated and washed several times with milliQ deionized water, until the washes has a conductivity equals to the conductivity of milliQ water (18,2 MΩ cm). An average diameter of 3 mm was obtained for chitosan gel beads. This measurement was obtained as an average of 100 diameter bead measurement performed with an optical microscope.

2.4. Statistical experimental design

An experimental screening design was used to identify the key factors that modified significantly the response. A Plackett- Burman design was performed (Bruns, Acarmino, & de Barros Neto, 2006). The factors studied were pH (pH = 1–12), sorbent dosage (m = 0.42–4.25 g L^{-1}), temperature (T = 20–60 °C) and contact time (t = 1–60 min), $[MoO_4^{2-}]_0$ = 2.0 mM; batch volume = 10.0 mL. From studied factors, sorbent dose and pH were significant ($P < 0.05$).

After the screening design, an optimization design was performed. The optimized model was achieved employing Central Composite Design (CCD) (Bezerra, Santelli, Oliveira, Villar, & Esclaleira, 2008). The factors studied were pH (pH = 1–12) and sorbent dosage (m = 0.42–6.65 g L^{-1}), $[MoO_4^{2-}]_0$ = 2.0 mM; batch volume = 10.0 mL. Once CCD was finished, a regression model was obtained for the response (mg Mo^{VI} sorbed/g chitosan). Analysis of variances (ANOVA) was applied to validate the model (See Table S1).

The variables used were pH and sorbent dosage, the number of repeat of each experiment was five, and the magnitude of the effects was: −2.75 pH (pointing to a decrease in sorption with an increase in pH values), +2.18 sorbent dose (pointing to an increase in sorption with an increase in sorbent doses values).

The relationship between Mo^{VI} removal (Y) and the test variables was:

$$Y = 16.50 - 2.75\ pH + 2.18\ sorbent\ dosage + 2.54\ (sorbent\ dosage)^2$$

The model F-value of 13.19 implies that the model is significant. Values of Prob > F less than 0.0500 indicate that the model terms are significant (see Table S1, Supplementary material). R^2 of this model is 0.8147, which is considered as having a high correlation. Therefore, it is reasonable to apply the model to analyze the trends of the responses.

The optimized model indicated that the highest removal of MoO_4^{2-} anions was achieved at pH 2.7 and sorbent dose = 5.40 g L^{-1}. Design Expert V. 7.0 software was used to mathematical calculations and statistical tests.

2.5. Batch adsorption experiments

Chitosan gel beads were suspended in solutions containing different amounts of Mo^{VI}. The polysaccharide dose was 5.40 ± 0.02 g L^{-1} at

pH 2.7. MoO_4^{2-} concentration was determined spectrophotometrically at 400 nm (Soni & Bartusek, 1971).

Kinetic and thermodynamic studies were performed in the 20–40 °C temperature range. Molybdate removal (q, mg g^{-1}) was calculated by Eq. (3):

$$q = \frac{(C_0 - C_t)V}{m} \quad (3)$$

where C_0 and C_t are the MoO_4^{2-} concentrations in solution (mg L^{-1}) at time 0 and t, respectively, V is the batch volume (L) and m is the quantity of chitosan used (g).

2.6. Continuous adsorption experiments

The adsorption of MoO_4^{2-} by chitosan packed in polypropylene columns of 15 cm long and 1.4 cm of internal diameter was studied. Powder Chitosan was previously equilibrated at pH 2.7, and packed by gravity into the columns keeping constant the package density. Upward flow of 9.0 mL min^{-1} was used. Solution containing 200 mg L^{-1} MoO_4^{2-} was pumped through the columns at pH 2.7 and room temperature. Samples of 2.0 mL were taken at different time intervals and MoO_4^{2-} concentration was measured. The adsorption capacity of molybdate ions was determined from Eq. (4).

$$q = \frac{C_0 Q}{1000m} \int_0^t (1 - \frac{C}{C_0})dt \quad (4)$$

where q is the mass of metal adsorbed (mg MoO_4^{2-} g chitosan^{-1}); C_0 is the intake solution concentration (mg L^{-1}); C the outtake solution concentration (mg L^{-1}); m is the amount of chitosan (g) and Q is the volumetric flow (mL min^{-1}).

The column bed performance was described through a breakthrough curve, which was obtained by plotting C/C_0 against time. Breakthrough time (t_b, min) was defined for an effluent MoO_4^{2-} concentration of 5.0 mg L^{-1}. Saturation time (t_{sat}, min) was considered when $C/C_0 = 0.95$.

Thomas model was applied to predict breakthrough curve behaviors. The expression of Thomas model is given in Eq. (5) (Thomas, 1944).

$$\frac{C}{C_0} = \frac{1}{1 + \exp\left(\frac{(q_{Th}m - C_0 vt)k_{Th}}{v}\right)} \quad (5)$$

where k_{Th} (L min^{-1} mg^{-1}) is Thomas rate constant, q_{Th} (mg g^{-1}) is the theoretical saturated adsorption capacity, v (L min^{-1}) is the flow rate and m (g) is the sorbent mass.

Modified dose–response model was also used (Yan, Viraraghavan, & Chen, 2001). Modified dose- response model is described by Eq. (6).

$$\frac{C}{C_0} = 1 - \frac{1}{1 + (\frac{vt}{b})^a} \quad (6)$$

where v (mL min^{-1}) is the flow rate. Parameters a and b comes from the modified dose–response model.

2.7. Real contaminated water analysis

Groundwater was collected from a hand pump attached tube well (depth: ~150 ft) of Buenos Aires State, Argentina and analyzed by standard methods (Clesceri, Greenberg, & Eaton, 1998). The parameters analyzed (mg L^{-1}) were total hardness (1778.51), calcium (492.81), sulphate (1285.7), phosphate (0.118), nitrate (40.3), nitrite (0.053), ammonia (0.00763), organic matter (1.96), total arsenic (0.00574), total chromium (0.2115), chromium(VI) (0.2110), molybdenum (VI) (less than 0.001) and pH (7.80). This water sample was spiked with molybdenum(VI) up to a level of desire (40.0 mg L^{-1}) for conducting experiments and the working pH was adjusted to 2.7. The employed bed depth was 0.9 cm with an upward flow of 9.0 mL min^{-1} groundwater.

Desorption studies employed 0.10 M solution of NaOH eluent and an upward flow of 2.0 mL min^{-1}. The adsorption–desorption cycles were repeated two times. Desorption efficiency was calculated using Eq. (7).

$$Desorption\ efficiency(\%) = \frac{mol\ Mo\ released}{mol\ Mo\ adsorbed} \times 100 \quad (7)$$

2.8. FT-IR, SEM/EDS analysis and thermogravimetric analysis (TGA)

Chitosan beads were obtained as described in Section 2.3. After washed, the beads were desiccated under vacuum for 48 h until constant mass was obtained. These beads were used in FT-IR, SEM/EDS and TGA experiments.

Molybdate loaded chitosan beads were obtained as described in Section 2.5. The content of molybdate was 255 mg molybdate/g chitosan beads. After washed, the beads were desiccated under vacuum for 48 h until constant mass was obtained. These beads were used in FT-IR, SEM/EDS and TGA experiments.

FT-IR spectra were measured using a Perkin Elmer FT-IR Spectrum One spectrophotometer in the range of 200–4000 cm^{-1} employing CsI pellets.

Surface structure of chitosan gel beads was analyzed by scanning electron microscopy (SEM) and Mo adsorbed on the chitosan beads was checked by EDS microanalysis. SEM analysis was performed by means of a FEI QUANTA 200F in low vacuum mode (0.20–0.40 mbar chamber pressure), working distance 10–12 mm, acceleration voltage 10–15 kV, on non coated samples. Before the analysis, chitosan beads were placed on aluminum stubs by using carbon adhesive disks. Energy Dispersive X-ray (EDS) analysis was performed on the above described SEM apparatus, using a EDAX Si/Li detector, in low vacuum mode, working distance 10 mm, acceleration voltage 30 kV. SEM and EDS analysis were performed at LM CCT Rosario Laboratory.

TGA were performed in Thermogravimetric equipment DTG-60H, Shimadzu, made in Japón. N/P 346-68700-93, atmosphere: air, flow rate: 50 mL min^{-1}, temperature range 30–650 °C, temperature rate: 10 °C/min, chitosan bead mass: 20.676 mg, molybdate loaded chitosan bead mass: 21.410 mg.

3. Results and discussion

3.1. Kinetic studies

Rate studies of adsorption processes allow design continuous bed adsorption systems (Hawari, Rawaifih, & Nsour, 2009). Pseudo first and pseudo second kinetic models were used in the present work to fit adsorption kinetic data.

The pseudo first-order kinetic model was expressed as shown in Eq. (8):

$$q_t = q_e\left(1 - e^{-k_1 t}\right) \quad (8)$$

where k_1 (min^{-1}) is the first-order-rate constant (Lagergren, 1898).

The pseudo second-order kinetic model was represented by Eq. (9):

$$q_t = \frac{t}{\left(\frac{1}{k_2 q_e^2} + \frac{t}{q_e}\right)} \quad (9)$$

where k_2 (min^{-1} g mg^{-1}) is the second-order-rate constant (Ho & McKay, 1999).

Fig. 1 showed experimental data and best fit employing both models at 20 °C.

The validity of the model was checked by correlation parameter (R^2) as well as the consistence between predicted and experimental

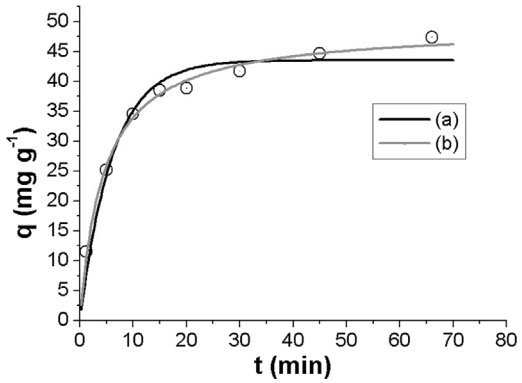

Fig. 1. Kinetic data and best fit employing pseudo first and second order kinetic models. Chitosan doses = 5.40 g L^{-1}; T = 20 °C; pH = 2.7; $[MoO_4^{2-}]_0$ = 2.02 m M; (a) first order kinetic model; (b) second order kinetic model.

values of q_e.

Taking into account the correlation coefficient values (R^2) and accordance between calculated and experimental q_e values, the pseudo-second order kinetic model is the better model to describe MoO_4^{2-} removal kinetic data. Table 1 resumes the values of k_1, k_2, q_e and correlation coefficients obtained at three temperature values.

Activation energy (E_a) of adsorption process was calculated from the slope of Arrhenius plot in its linealized form (Bertoni et al., 2015), (see Fig. S2, Supplementary material).

The value of E_a was 8.8 kJ mol^{-1}. In physical adsorption, sorbate-sorbent equilibrium is rapidly attained and easily reversible, due to forces involved in the process are weak. E_a values for physical adsorption are usually lower than 4.184 kJ mol^{-1}, E_a value obtained in the present work is in agreement with a chemisorption mechanism (Blanes et al., 2016; Bertoni et al., 2015).

3.2. Adsorption isotherms

Adsorption isotherms were used to describe the equilibrium adsorbate- adsorbent and free adsorbate in aqueous phase. Four isotherm models were used in the present work.

Langmuir isotherm model is given by Eq. (10) (Langmuir, 1918):

$$q_e = \frac{q_m K_L C_e}{1 + K_L C_e} \tag{10}$$

where C_e is the equilibrium concentration of sorbate (mg L^{-1}), K_L is the Langmuir equilibrium constant, and q_m is the amount of sorbate required to form a monolayer onto the sorbent surface (mg kg^{-1}). Separation factor, R_L, calculated using Eq. (11) (Weber & Chakravorti, 1974), was used to verified the correct application of the Langmuir isotherm model.

$$R_L = \frac{1}{1 + K_L C_0} \tag{11}$$

Table 1
Kinetic parameters and coefficients of determination (R^2).

	T 20 °C	T 30 °C	T 40 °C
Pseudo-first order			
q_e (mg g^{-1})	43 ± 1	50 ± 1	49 ± 1
k_1 (min^{-1})	0.16 ± 0.02	0.26 ± 0.03	0.27 ± 0.02
R^2	0.9543	0.9638	0.9839
Pseudo-second order			
q_e (mg g^{-1})	49.1 ± 0.9	57 ± 1	56.1 ± 0.6
k_2 (g min^{-1} mg^{-1})	0.0046 ± 0.0004	0.0052 ± 0.0003	0.0058 ± 0.0004
R^2	0.9926	0.9917	0.9974

Chitosan doses 5.40 g L^{-1}; pH = 2.7; $[MoO_4^{2-}]_0$ = 2.02 mM.

where C_o is the highest molybdate concentration (mol L^{-1}). Adsorption process is favourable when R_L values lie between 0 and 1.

Freundlich isotherm model is given by Eq. (12) (Freundlich, 1906).

$$q_e = K_F C_e^{1/n} \tag{12}$$

where K_F and $1/n$ are the Freundlich equilibrium constant and the coefficient of heterogeneity, respectively.

Sips isotherm model was applied in order to determine if Langmuir or Freundlich model was the most adequate isotherm model (Sips, 1948). Sips isotherm model is expressed by Eq. (13).

$$q_e = \frac{q_m b C_e^N}{1 + b C_e^N} \tag{13}$$

where q_m is the amount of sorbate required to form a monolayer (mg g^{-1}), b is the Sips constant and N is the Sips exponent.

The Dubinin- Radushkevich (D-R) isotherm model is given by Eq. (14) (Dubinin & Radushkevich, 1947).

$$q_e = q_m e^{-\beta \varepsilon^2} \tag{14}$$

where β is a constant (mol^2 J^{-2}), q_m the theoretical saturation capacity, and ε is the Polanyi potential, which is equal to RT ln(1 + (1/Ce)), R (J mol^{-1} K^{-1}) is the gas constant and T (K) is the absolute temperature.

The mean free energy E (kJ mol^{-1}) of adsorption is related to the constant β and can be calculated using Eq. (15) (Dubey & Gupta, 2005).

$$E = \frac{1}{(2\beta)^{1/2}} \tag{15}$$

E values between 8 and 16 kJ mol^{-1}, pointed out the adsorption mechanism is chemical adsorption, while for the values of E < 8 kJ mol^{-1}, the adsorption process follows physical mechanism (Blanes et al., 2016; Bertoni et al., 2015). Values of mean free energy of adsorption at different temperature values and the various constants of the isotherm models were tabulated in Table 2.

E values were in the range 8.8–11.2 kJ mol^{-1}, supporting that adsorption process follows chemical mechanism.

The maximum adsorption capacity increases at higher T values, which could be explained as an increment in the number of exposed adsorption sites due to changes in polysaccharide conformation with temperature leading to more adsorption sites becoming accessible to molybdate ions. Data obtained were fitted well with Langmuir model at the three temperature values studied. Sips exponent (N) was quite close to unity at the three temperature values. This implied that the use of Langmuir isotherm model for this adsorption system is appropriate. The R_L values showed that the adsorption process was favorable ($0 < R_L < 1$).

Adsorption capacity of chitosan polysaccharide was contrasted with other adsorbents reported in literature, see Table 3.

Chitosan has a high adsorption capacity and it was comparable with other sorbents. Reported magnetic chitosan resin possess a higher uptake capability because the presence of magnetite in their structure offers more binding sites to molybdate anions and increment the net positive charge of the resin resulting in an improve in its uptake capability.

Therefore, considering the low commercial value of this natural polysaccharide, it is a good alternative to be employed in groundwater and wastewater treatment.

Experimental data of Mo^{VI} adsorption at various temperature values and best fit of Langmuir model are shown in Fig. 2.

From Fig. 2 it can be seen that an increment in temperature produces an increment in the qmax value. This trend can be explained by considering that the adsorption process under studied was endothermic. Also the good fitting of Langmuir model suggests that the binding sites in the surface are equals and the molybdate anions forms a monolayer over the chitosan bead surface.

Table 2
Characteristic parameters of the different isotherm models and coefficients of determination (R^2).

	T 20 °C	T 30 °C	T 40 °C
Langmuir			
q_m (mg g^{-1})	265 ± 1	387 ± 3	474 ± 1
K_L (L mg^{-1})	0.0136 ± 0.0007	0.0062 ± 0.0007	0.0038 ± 0.0005
R_L	0.030	0.064	0.100
R^2	0.9957	0.9896	0.9896
Freundlich			
K_F	33 ± 6	18 ± 4	19 ± 3
1/n	0.32 ± 0.03	0.46 ± 0.04	0.59 ± 0.06
R^2	0.9397	0.9667	0.9616
Sips			
q_m	250 ± 1	400 ± 3	390 ± 1
b	0.006 ± 0.001	0.005 ± 0.003	0.0018 ± 0.0009
N	1.22 ± 0.06	1.1 ± 0.2	1.2 ± 0.1
R^2	0.9987	0.9898	0.9934
D-R			
q_m (mg g^{-1})	520 ± 50	1000 ± 100	1300 ± 200
β (mol^2 J^{-2}) × 10^9	4.0 ± 0.4	5.4 ± 0.4	6.4 ± 0.5
E (kJ mol^{-1})	11.2 ± 0.1	9.62 ± 0.03	8.84 ± 0.02
R^2	0.9588	0.9777	0.9759

Chitosan doses 5.40 g L^{-1}; pH = 2.7; $[MoO_4^{2-}]_0$ = 320–2360 mg L^{-1}.

Table 3
Adsorption of MoO_4^{2-} ions by chitosan and other sorbents reported in literature.

Sorbent	MoO_4^{2-} uptake (mg g^{-1})	Reference
Organo-bentonite	224	Dodbiba et al. (2011)
Goethite	25.9	Elwakeel, Atia, and Donia (2009)
Green seaweed	1280	Bertoni et al. (2015)
Fe(III)-orange peel gel	176	Faghihian, Malekpour, and Maragheh (2002)
Magnetic chitosan resin	1280	Wu, Lo, and Lin (2000)
Hematite	10.39	Xu, Christodoulatos, and Braida (2006)
Chitosan gel bead	265	This work

3.3. Adsorption thermodynamics

Thermodynamic parameters such as enthalpy change (ΔH°), entropy change (ΔS°) and free energy change (ΔG°) are useful to describe the spontaneity of a process.

The adsorption free energy change, ΔG°, is known by Eq. (16) (Blanes et al., 2016; Bertoni et al., 2015).

$$\Delta G^\circ = -RT \ln 55.5\, K_L \quad (16)$$

Where: K_L is the Langmuir constant (L mol^{-1}), 55.5 is the water molarity (mol L^{-1}), R is the universal gas constant (8.314 J mol^{-1} K^{-1}), and T is the absolute temperature (K).

The heat of adsorption of the sorbent, ΔH° (kJ mol^{-1}), and entropy ΔS° (J mol^{-1} K^{-1}) for the adsorption process can be calculated by Eq. (17) (Blanes et al., 2016; Bertoni et al., 2015).

$$\ln 55.5K_L = \frac{\Delta S^\circ}{R} - \frac{\Delta H^\circ}{R}\frac{1}{T} \quad (17)$$

The obtained thermodynamic were ΔH° = −49.1 kJ mol^{-1} and ΔS° = 66.5 J K^{-1} mol^{-1}.

The exothermic adsorption processes imply that a release of energy occurs after binding of molybdate ions to the chitosan surface. Negative ΔS° values showed that an increase of the system order occurs. The negative values of ΔG° pointed out to the spontaneity of the studied adsorption process.

3.4. FTIR analysis and surface characterization

FTIR spectra of chitosan gel beads, before and after MoO_4^{2-} binding, were used to find out the functional groups responsible for molybdate ions binding. The spectra were measured in the range of 200–4000 cm^{-1} employing CsI pellets (Fig. 3).

Table S2 resumes major stretching vibrations of chitosan polysaccharide and chitosan- molybdate.

After MoO_4^{2-} binding by the polysaccharide, some changes in the FT-IR spectra arise. Stretching vibration corresponding to Mo═O and Mo−O bond appeared (904 cm^{-1} and 695 cm^{-1}, respectively). The signal to Mo−O−Mo (838 cm^{-1}), suggest that polynuclear species of Mo^{VI} are present at the surface of chitosan gel beads (Bertoni et al., 2015). The signal assigned to O−H stretching (Pérez Marín et al., 2009) was shifted and the C−O vibration was strengthened and shifted. No vibrations corresponding to Mo-N was observed (ν_{st} Mo−N: 470 cm^{-1}). This experimental observation suggest that active surface sites are composed only by oxygenated groups. These results suggest that hydroxyl groups participate in binding of molybdate anions onto the surface of the polysaccharide.

Scanning electron microscope (SEM) images were used for chitosan gel beads surface analysis (see Fig. S3, Supplementary material). Fig. S3A showed the chitosan gel bead as a whole, and Fig. S3B showed the surface structure of this bead. The dehydrated gel bead is a spherical particle with an approximate 1.8 mm diameter. The surface presented reliefs in a lineal arrangement on the surface. After MoO_4^{2-} adsorption, the dehydrated gel bead retains its spherical form with an approximate 1.5 mm diameter (see Fig. S3C Supplementary material). The surface suffers some changes: the reliefs were shorter and the distribution of the same was irregular (see Fig. S3 D). Changes in the surface morphology after MoO_4^{2-} adsorption indicate that the surface polysaccharide chains suffer a rearrangement during the adsorption process. These changes were observed in others systems reported in literature (Bertoni et al., 2015; Blanes et al., 2016; Murphy, Tofail, Hughes, & McLoughlin, 2009).

EDS analysis of chitosan gel beads after molybdate removal, displayed a signal corresponding to Mo k signal at 17.3 keV (see Fig. S4A–C), confirming that molybdenum was bonded to the surface of chitosan. EDS measurement was performed at three different portion of the gel bead surface in order to obtain an average content of Mo. The average Mo content was 15.1% Mo. This value corresponds to a molybdate load of 252 mg/g chitosan gel bead, which was in agreement

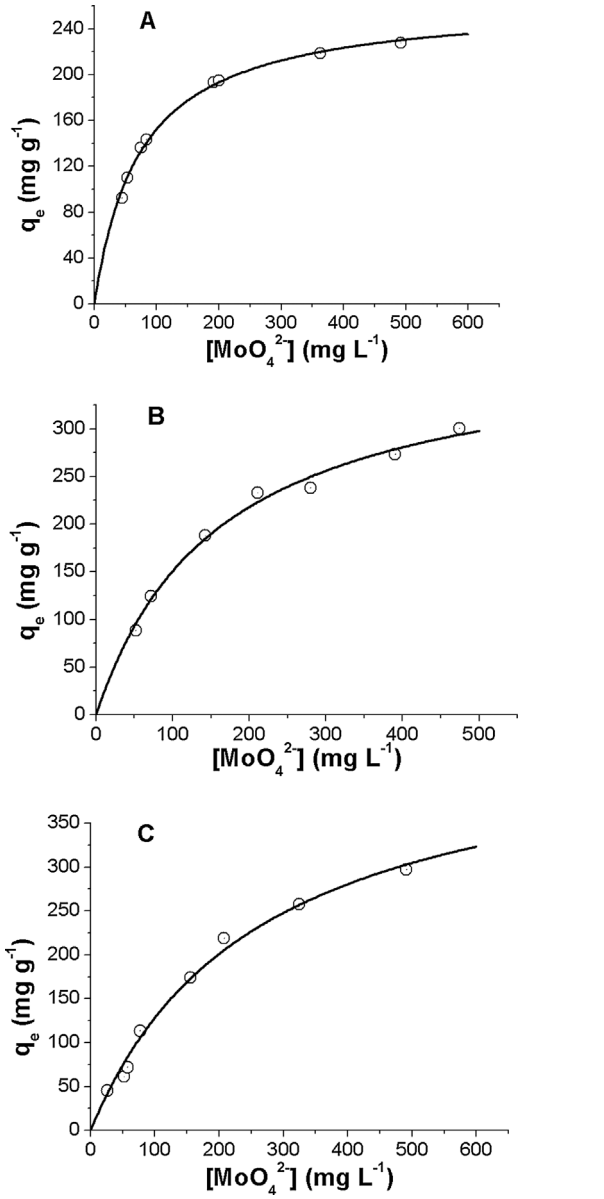

Fig. 2. Adsorption isotherm of molybdate ions onto chitosan gel beads. Polysaccharide doses = 5.40 g L^{-1}; pH = 2.7; [MoO_4^{2-}]$_0$ = 10–600.00 mg L^{-1}. (A) 20 °C; (B) 30 °C; (C) 40 °C. (—) Langmuir Model.

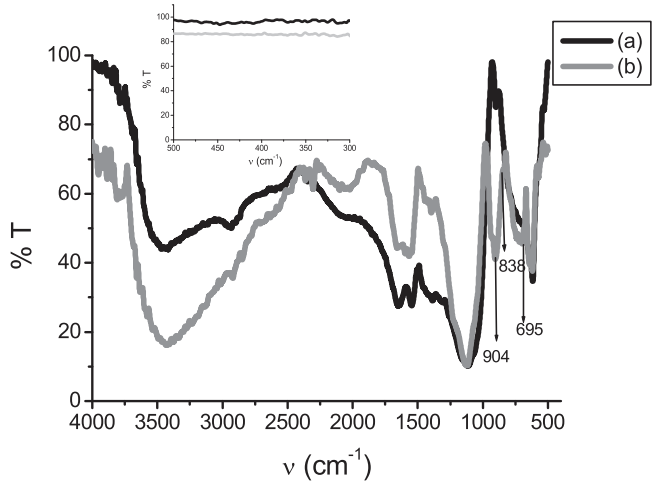

Fig. 3. FT-IR spectra of: (a) Chitosan; (b) Chitosan-Molybdate.

with the experimental value q = 255 mg/g of the used chitosan gel beads loaded with Mo in this experiment.

EDS mapping showed a uniform surface distribution of molybdate ions onto chitosan gel beads (see Fig. S5).

In order to improve the chemico-physical characterization of the system, it was performed thermogravimetric analysis (TGA), of chitosan beads and molybdate loaded chitosan beads (see Fig. S6).

Chitosan thermogram showed a loss of water in the range 100–200 °C (19% mass loss) and decomposition of the polymer in the range 200- 300 °C (51% mass loss). This behavior was expected by chitosan polymer and it was reported previously in literature (Abdou et al., 2008). Chitosan loaded thermogram showed a different behavior. The loss of water occurs in the range 100–210 °C (17% mass loss) but decomposition of the polymer occurs in the range 220–350 °C (29% mass loss). This results points to chitosan beads loaded with molybdate had a better thermal stability than chitosan beads.

The resultant residue represents a higher percent of total polymer mass (39% in chitosan beads loaded with molybdate against 20% in chitosan beads). This increment in residue mass was due to presence of sodium molybdate in the residue.

Presence of about 19% of sodium molybdate in the residue is in accordance to the original content of molybdate in the beads (255 mg molybdate/g chitosan bead) and supports the results obtained by EDS analysis.

Taking into account the results obtained in the present work we proposed in Scheme 1, a mechanism for molybdate binding to chitosan polysaccharide.

Presence of polynuclear heptamolybdate anions and participation of hydroxyl functional groups as active binding sites, were proposed based on IR evidence.

Amino group of chitosan was protonated at working pH (2.7) so, the coordination capability of this group was blocked. Coordination of molybdate anions with hydroxyl groups of sugar residues was previously reported in literature (Matulová, Verchere, & Chapelle, 1996; Sauvage, Verchere, & Chapelle, 1996) Our results support the coordination of molybdate anions to hydroxyl groups of chitosan. The proposed role of protonated amino group was stabilization of negative charged heptamolybdate anions to the surface. Electrostatic interaction between protonated amino groups plus binding of heptamolybdate anions to hydroxyl groups of chitosan results in the retention of molybdate by chitosan beads.

3.5. Fixed bed column studies

Breakthrough curves at three values of bed heights and Modified dose–response model best fit are plotted in Fig. 4.

MoO_4^{2-} ions uptake (mg g^{-1}), breakthrough and saturation time obtained experimentally were listed in Table S3. Table S4 showed the parameters of both mathematical models, and the correlation coefficients (R^2).

The values of q_{Th} were in agreement with the experimental q values. q_{Th} values were higher than the q_{max} obtained in batch experiments. These results are a consequence of the higher exposed surface of chitosan in column experiments. The values of k_{Th} decreases as bed height increases, suggesting that kinetic became slower at higher column heights values. This trend in k_{Th} values with respect to column bed height was previously reported in literature (Song, Zou, Bian, Su, & Han, 2011).

Experimental data were better described by modified dose response model. R^2 values increases to 0.993–0.997 showing an excellent fit of the experimental data. The values of parameter b increased at high values of bed height. This trend was previously reported in literature (Bertoni et al., 2015).

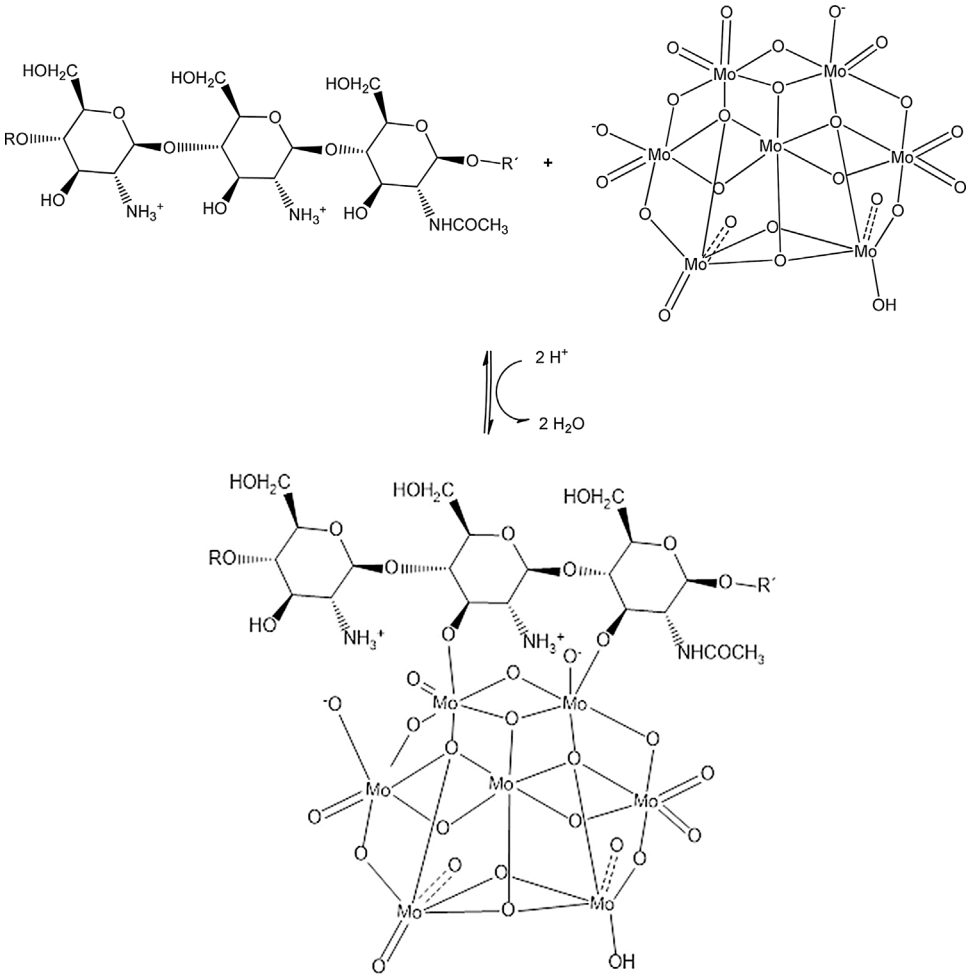

Scheme 1. Proposed mechanism for Mo^{VI} binding to chitosan polysaccharide.

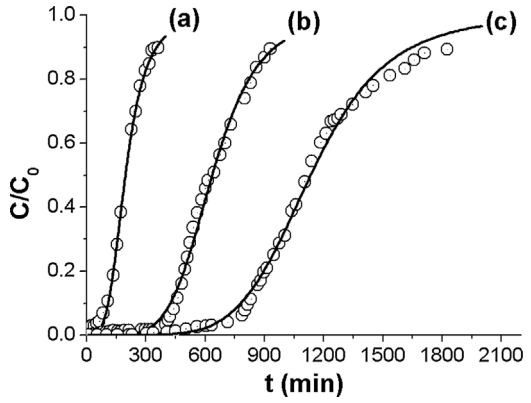

Fig. 4. Breakthrough curves and Modified doses- response models for different bed heights. C_0 = 200.0 mg L^{-1} MoO_4^{2-}; Q = 9.0 mL min^{-1}; T = 20 °C; pH = 2.7. (a) h = 0.9 cm; (b) h = 2.5 cm; (c) h = 4.1 cm.

3.6. Scale-up studies

Scale-up studies were performed applying the bed depth service time (BDST) model (Bohart & Adams, 1920).

Eq. (18) expresses a linear function of the operation time with the bed depth:

$$t = \frac{N_0}{C_0 v} Z - \frac{1}{k_{BDST} C_0} \ln\left(\frac{C_0}{C} - 1\right) \quad (18)$$

where N_0 is the adsorption capacity (mg L^{-1}), v is the fluid velocity (cm min^{-1}) and k_{BDST} is the kinetic constant (L mg^{-1} min^{-1}).

Iso-concentration lines for MoO_4^{2-} anions adsorption in a fixed bed at four C/C_0 ratios were calculated, (see Fig. S7). Table S5 showed the k_{BDST} and N_0 parameters obtained for different C/C_0 ratios.

N_o values at low breakthrough condition were lower than the full bed capacity of the biomass because on the chitosan surface, some active sites remain free at lower C_t/C_0 ratio value (Bohart & Adams, 1920). The rate constant, k_{BDST}, remains equals in the C_t/C_0 range employed.

BDST model was validated by inspection of breakthrough curve at 50%. In this condition, the logarithmic term is equal to zero. Good fitting was achieved at 50% breakthrough validating the application of BDST model to the adsorption process of MoO_4^{2-} by chitosan polysaccharide. The critical bed depth, Z_0 is obtained by Eq. (19).

$$Z_0 = \frac{v}{k_{BDST} N_0} \ln\left(\frac{C_0}{C_b} - 1\right) \quad (19)$$

The critical bed depth, Z_o was equals to 0.77 cm. This value corresponds to the minimum theoretical bed height of chitosan that produces an effluent concentration at t = 0 lower than breakthrough concentration.

3.7. Real sample analysis

Ultimately, we tested chitosan as an adsorbent for molybdate ions into contaminated groundwater. Adsorbent reusability was checked by conducting two-adsorption–desorption cycles. The breakthrough time (tb) was 160 min and the volume of water treated (Vb) at breakthrough was 1.44 L in the first cycle. Due to the high affinity of chitosan towards

Cr^{VI} species at pH 2.7 (also present in groundwater sample), Cr^{VI} removal from groundwater was studied. A removal of 100% Cr^{VI} was achieved during the two cycles.

Desorption/recovery of molybdate from the column was performed with 0.1 M NaOH solution. It was observed that the percentage (%) of MoO_4^{2-} desorption was 100% and the percentage (%) of Cr^{VI} desorption was 0% in the first cycle. The volume of desorption solution employed was 0.09L. Molybdenum breakthrough time (tb) decreased to 55 min in the second cycle (over 75% loss of removal capacity). Loss of removal capacity was probably due to Cr^{VI} kept strongly bonded to chitosan blocking active sites for Mo^{VI} removal. The effluent water quality suggests that the molybdenum removed water by chitosan could be used for household purposes.

4. Conclusions

We report the application of chitosan polymer, as a sorbent of Mo^{VI} ions. Participation of hydroxyl groups in binding of Mo^{VI} anions at the surface of chitosan gel beads was confirmed by FT-IR analysis. Kinetic and thermodynamic parameters confirm that the removal mechanism was chemical adsorption. Continuous adsorption data were analyzed applying three models. Application of chitosan in molybdate removal from real groundwater samples suggest that this polysaccharide is a good option to be used for household purposes. The high value of q_{max} and the low cost of this polysaccharide make this biomass a good sorbent for being used in continuous treatment of groundwater and effluents contaminated with molybdate anions.

Acknowledgements

We thank the National Research Council of Argentina (CONICET) PIP 0037, National Agency of Scientific and Technological Promotion (ANPCyT)PICT 2014-0529 and National University of Rosario (UNR) BIO344, BIO425 for financial support.

Appendix A. Supplementary data

Supplementary data associated with this article can be found, in the online version, at http://dx.doi.org/10.1016/j.carbpol.2017.10.027.

References

Abdou, E., Nagy, K., & Elsabee, M. (2008). Extraction and characterization of chitin and chitosan from local sources. *Bioresource Technology, 99*, 1359–1367.
Bei, H., Shim, S., George, E., Miller, M., Herbert, H., & Pharr, G. (2007). Compressive strengths of molybdenum alloy micro-pillars prepared using a new technique. *Scripta Materialia, 57*, 397–400.
Beil, S., Schamberger, A., Naumann, W., Machill, S., & van Pée, K. (2012). Determination of the degree of N-acetylation (DA) of chitin and chitosan in the presence of water by first derivative ATR FTIR spectroscopy. *Carbohydrate Polymers, 87*, 117–122.
Bertoni, F. A., Medeot, A. C., Gonzalez, J. C., Sala, L. F., & Bellu, S. E. (2015). Application of green seaweed biomass for Mo^{VI} sorption from contaminated waters. Kinetic, thermodynamic and continuous sorption studies. *Journal of Colloid and Interface Science, 446*, 122–132.
Bezerra, M. A., Santelli, R. E. E., Oliveira, P., Villar, L. S., & Esclaleira, L. A. (2008). Response surface methodology (RSM) as a tool for optimization in analytical chemistry. *Talanta, 76*, 965–977.
Blanes, P. S., Bordoni, M. E., González, J. C., García, S. I., Atria, A. M., Sala, L. F., et al. (2016). Application of soy hull biomass in removal of Cr(VI) from contaminated waters. Kinetic, thermodynamic and continuous sorption studies. *Journal of Environmental Chemical Engineering, 4*, 516–526.
Bof, M. J., Bordagaray, V. C., Locaso, D. E., & García, M. A. (2015). Chitosan molecular weight effect on starch-composite film properties. *Food Hydrocolloids, 51*, 281–294.
Bohart, G. S., & Adams, E. Q. (1920). Behavior of charcoal towards chlorine. *Journal of the Chemical Society, 42*, 523–529.
Bruns, R. E., Scarmino, I. S., & de Barros Neto, B. (2006). *Statistical design-chemometrics* (1st ed.). Amsterdam: Elsevier.
Clesceri, L. S., Greenberg, A. E., & Eaton, A. D. (1998). *Standard methods for the examination of water and wastewater analysis* (21st ed.). Washington, DC: APHA, AWWA, WEF.
Dodbiba, G., Fujii, T., Kikuchi, T., Manjanna, J., Matsuo, S., Takahashi, H., et al. (2011). Synthesis of iron-based adsorbents and their application in the adsorption of molybdenum ions in nitric acid solution. *Chemical Engineering Journal, 166*, 496–503.
Dubey, S. S., & Gupta, R. K. (2005). Removal behavior of Babul bark (Acacia nilotica) for submicro concentrations of Hg^{2+} from aqueous solutions: A radiotracer study. *Separation and Purification Technology, 41*, 21–28.
Dubinin, M. M., & Radushkevich, L. V. (1947). Equation of the characteristic curve of activated charcoal. *Proceedings of the Academy of Sciences, Physical Chemistry Section, 55*, 331–333.
Elwakeel, K., Atia, A., & Donia, A. (2009). Removal of Mo(VI) as oxoanions from aqueous solutions using chemically modified magnetic chitosan resins. *Hydrometallurgy, 97*, 21–28.
Faghihian, H., Malekpour, A., & Maragheh, M. G. (2002). Adsorption of molybdate ion by natrolite and clinoptilolite-rich tuffs. *International Journal of Environment and Pollution, 18*, 181–189.
Freundlich, H. M. F. (1906). Over the adsorption in solution. *Zeitschrift fur Physikalische Chemie, 57*, 385–470.
Fu, F., & Wang, Q. (2011). Removal of heavy metal ions from wastewaters: A review. *Journal of Environmental Management, 92*, 407–418.
Goldberg, S., Lesch, S. M., & Suarez, D. L. (2002). Predicting molybdenum adsorption by soils using soil chemical parameters in the constant capacitance model. *Soil Science Society of America Journal, 66*, 1836–1842.
Guibal, E. (2004). Interactions of metal ions with chitosan-based sorbents: A review. *Separation and Purification Technology, 38*(1), 43–74.
Gupta, U. C. (1997). Symptoms of molybdenum deficiency and toxicity in crops. In U. C. Gupta (Ed.). *Molybdenum in agriculture* (pp. 160–170). Cambridge University Press.
Hawari, A., Rawajfih, Z., & Nsour, N. (2009). Equilibrium and thermodynamic analysis of zinc ions adsorption by olive oil mill solid residues. *Journal of Hazardous Materials, 168*, 1284–1289.
Hirai, H., Odani, H., & Nakajima, A. (1991). Determination of degree of deacetylation of chitosan by 1H NMR spectroscopy. *Polymer Bulletin, 26*, 87–94.
Ho, Y. S., & McKay, G. (1999). Pseudo-second order model for sorption processes. *Process Biochemistry, 34*, 451–465.
Hua, C., Zhang, R., Bai, F., Lu, P., & Liang, X. (2017). Removal of chromium (VI) from aqueous solutions using quaternized chitosan microspheres. *Chinese Journal of Chemical Engineering, 25*, 153–158.
Kumar, A., & Jiang, S. (2016). Chitosan-functionalized graphene oxide: A novel adsorbent an efficient adsorption of arsenic from aqueous solutions. *Journal of Environmental Chemical Engineering, 4*, 1698–1713.
Lagergren, S. (1898). About the theory of so-called adsorption of soluble substances. *Handlingar, 24*, 1–39.
Langmuir, I. (1918). The adsorption of gases on plane surfaces of glass, mica and platinum. *Journal of the American Chemical Society, 40*(9), 1361–1403.
Li, K., Li, P., Cai, J., Xiao, S., Yang, H., & Li, A. (2016). Efficient adsorption of both methyl orange and chromium from their aqueous mixtures using a quaternary ammonium salt modified chitosan magnetic composite adsorbent. *Chemosphere, 154*, 310–318.
Mallakpour, S., & Madani, M. (2016). Functionalized-MnO2/chitosan nanocomposites: A promising adsorbent for the removal of lead ions. *Carbohydrate Polymers, 147*, 53–59.
Matulová, M., Verchere, J., & Chapelle, S. (1996). Furanose vs. acyclic forms of carbohydrate ligands. A multinuclear NMR spectroscopy study of the molybdate and tungstate complexes of D-g lycero-L-manno-heptose. *Carbohydrate Research, 287*, 37–48.
Moret, A., & Rubio, J. (2003). Sulphate and molybdate ions uptake by chitin-based shrimp shells. *Journal of Mineral Engineering, 16*, 715–722.
Murphy, V., Tofail, S., Hughes, H., & McLoughlin, P. (2009). A novel study of hexavalent chromium detoxification by selected seaweed species using SEM-EDX and XPS analysis. *Chemical Engineering Journal, 148*, 425–433.
Pérez Marín, A. B., Aguilar, M. I., Meseguer, V. F., Ortuño, M. F., Sáez, J., & Lloréns, M. (2009). Biosorption of chromium (III) by orange (*Citrus cinensis*) waste: Batch and continuous studies. *Chemical Engineering Journal, 155*, 199–206.
Padilla-Rodriguez, A., Hernandez-Viezcas, J., Peralta-Videa, J., Gardea-Torresdey, J., Perales-Perez, O., & Roman-Velazques, F. (2015). Synthesis of protonated chitosan flakes for the removal of vanadium(III, IV and V) oxyanions from aqueous solutions. *Microchemical Journal, 118*, 1–11.
Roberts, G. A. F., & Domszy, J. G. (1982). Determination of the viscosimetric constants for chitosan. *International Journal of Biological Macromolecules, 4*, 374–377.
Sauvage, J., Verchere, J., & Chapelle, S. (1996). A multinuclear NMR spectroscopy study of the tungstate and molybdate complexes of D-fructose and L-sorbose. *Carbohydrate Research, 286*, 67–76.
Sips, R. (1948). On the structure of a catalyst surface. *Journal of Chemical Physics, 16*, 490–495.
Smedley, P., Nicolli, H., Macdonald, D., Barros, A., & Tullio, J. (2002). Hydrogeochemistry of arsenic and other inorganic constituents in groundwater from La Pampa, Argentina. *Applied Geochemistry, 17*, 259–284.
Song, J., Zou, W., Bian, Y., Su, F., & Han, R. (2011). Adsorption characteristics of methylene blue by peanut husk in batch and column modes. *Desalination, 265*, 119–125.
Soni, R., & Bartusek, M. (1971). Molybdate complexes with *o*-diphenols. *Journal of Inorganic and Nuclear Chemistry, 33*, 2557–2563.
Thomas, H. C. (1944). Heterogeneous ion exchange in a flowing system. *Journal of the American Chemical Society, 66*, 1664–1666.
Weber, T. W., & Chakravorti, R. K. (1974). Pore and Solid diffusion models for fixed bed adsorbers. *Journal of American Institute of Chemical Engineers, 20*, 228–238.
Wu, C. H., Lo, S. L., & Lin, C. F. (2000). Competitive adsorption of molybdate, chromate, sulfate, selenate, and selenite on γ-Al_2O_3. *Colloids and Surfaces A: Physicochemical and Engineering Aspects, 166*, 251–259.
Xu, N., Christodoulatos, C., & Braida, W. (2006). Adsorption of molybdate and tetrathiomolybdate onto pyrite and goethite: Effect of pH and competitive anions. *Chemosphere, 62*, 1726–1735.
Yan, G., Viraraghavan, T., & Chen, M. (2001). A new model for heavy metal removal in a biosorption column. *Adsorption Science & Technology, 19*, 25–43.